

DOI: 10.1070/QE2016v046n01ABEH015867

Formation of a fine-dispersed liquid-metal target under the action of femto- and picosecond laser pulses for a laser-plasma radiation source in the extreme ultraviolet range

A.Yu. Vinokhodov, K.N. Koshelev, V.N. Krivtsun, M.S. Krivokorytov, Yu.V. Sidelnikov, V.V. Medvedev, V.O. Kompanets, A.A. Melnikov, S.V. Chekalin

Abstract. **We report the results of studying the dynamics of deformation and fragmentation of liquid-metal droplets under the action of ultrashort laser pulses. The experiments have been performed to optimise the shape of the droplet target used in extreme ultraviolet (EUV) radiation sources based on the laser-produced plasma using the pre-pulse technology. The pre-pulse is generated by a system incorporating a master Ti:sapphire oscillator and a regenerative amplifier, allowing one to vary the pulse duration from 50 fs to 50 ps. The power density of laser radiation at the droplet target, averaged over the pulse duration and spatial coordinates, has reached 3×10^{15} W cm^{-2}. The production of liquid-metal droplets has been implemented by means of a droplet generator based on a nozzle with a ring piezoceramic actuator. The droplet material is the eutectic indium–tin alloy. The droplet generator could operate in the droplet and jet regime with a maximal rate of stable operation 5 and 150 kHz, respectively. The spatial stability of droplet position $\sigma = 1\%–2\%$ of its diameter is achieved. The size of the droplets varied within 30–70 μm, their velocity was 2–8 m s^{-1} depending on the operation regime.**

Keywords: *EUV lithography, source of EUV radiation, laser plasma, pre-pulse, femtosecond laser, droplet generator, laser target, liquid-metal droplets, repetitively pulsed regime.*

1. Introduction

Rapid development of the studies of plasma sources of radiation in the extreme ultraviolet (EUV) range observed in recent years was caused by their applications at the wavelength 13.5 nm in the new generation of lithography systems used to produce microchips with the characteristic scale smaller than 22 nm [1]. The competition of plasma sources of EUV radiation with the parameters required for industrial lithography that occurred during the recent few years [2] has shown the technological advantage of laser-plasma sources. In these sources, the role of a laser target is played by droplets of melted tin, generated with the frequency of a few tens of kilohertz and flying with the velocity of tens of metres per second. One of the technologies used in EUV laser sources based on droplet targets is the method of a laser pre-pulse [3] that allows the deformation of the droplet and its disintegration into small fragments. The size of such a target better matches the caustic size of the focused radiation of the main CO_2 laser. Besides, such fine-dispersed targets absorb laser radiation more efficiently, which, first increases the efficiency of its conversion into the EUV radiation, and, second, allows more efficient 'burning' of the target with laser radiation, i.e., significant reduction of the amount of 'unburned' target fragments, which essentially affect the lifetime of the optical system elements of the source. When a pulse from the Nd:YAG laser with a the duration 8 ns is used as a pre-pulse, the spherical target is deformed into a two-dimensional disk-shaped target [4]; for a laser pulse duration of 10 ps the droplet is deformed into a three-dimensional thin-wall dome-shaped structure. As the experiments [4] have shown, the latter allows generation of EUV radiation with a significantly higher conversion efficiency (CE) approaching $5\%/2\pi$ sr in the required spectral range, as well as more efficient 'burning' of the target fragments.

Thereupon, in the studies of the droplet target deformation dynamics and fine-dispersed target formation it is of undoubted scientific and practical interest to carry out comparative experiments with different pulse durations in the femto- and picosecond ranges. The purpose of the present work was to study the formation of a fine-dispersed target in the process of interaction between the droplet target and the laser radiation of femto- and picosecond range, to elaborate the diagnostic technique for the dynamics of droplet target expansion and to investigate different methods of synchronising the target formation and its irradiation with laser light, aimed at possible applications in the EUV sources based on laser plasma. The main method of diagnostics of the target formation process used in this work was photographing the shadow image of the droplet with short-time exposure and variable delay with respect to the laser pulse.

2. Experimental setup

The experimental setup is schematically shown in Fig. 1. Its major elements are the generator of liquid-metal droplets, the vacuum chamber and the femtosecond laser. The droplet generator is shown by the dashed circle in the centre of the vacuum chamber; the velocity vector of the droplets is directed orthogonally to the plane of the figure. The setup incorporates also the equipment for (i) synchronising the droplet formation and the laser pulse impact on it, (ii) diagnostics of the

A.Yu. Vinokhodov, M.S. Krivokorytov 'EUV Labs' Ltd., Sirenevyi blvd. 1, Troitsk, 142190 Moscow, Russia; e-mail avinokhod@gmail.com;
K.N. Koshelev, V.N. Krivtsun, Yu.V. Sidelnikov, V.V. Medvedev 'EUV Labs' Ltd., Sirenevyi blvd. 1, Troitsk, 142190 Moscow, Russia; Institute of Spectroscopy, Russian Academy of Sciences, ul. Fizicheskaya 5, Troitsk, 142190 Moscow, Russia; e-mail: krivtsun@isan.troitsk.ru;
V.O. Kompanets, A.A. Melnikov, S.V. Chekalin Institute of Spectroscopy, Russian Academy of Sciences, ul. Fizicheskaya 5, Troitsk, 142190 Moscow, Russia; e-mail: kompanetsvo@isan.troitsk.ru

Received 29 May 2015; revision received 6 October 2015
Kvantovaya Elektronika **46** (1) 23–28 (2016)
Translated by V.L. Derbov

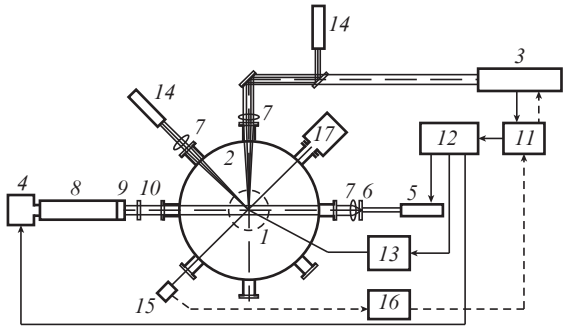

Figure 1. Schematic diagram of the setup:
(*1*) droplet generator; (*2*) vacuum chamber; (*3*) femtosecond laser; (*4*) CCD video camera; (*5*) transilluminating diode laser; (*6*) optical diffuser; (*7*) focusing lenses; (*8*) microscope; (*9*) objective; (*10*) narrow-band filter; (*11*) delay generator; (*12*) frequency divider; (*13*) control unit of the droplet generator; (*14*) continuous-wave visible-range lasers; (*15*) photodiode with a transimpedance amplifier; (*16*) detector of the signal maximum; (*17*) Faraday cylinder.

droplet and its fragments and (iii) ion diagnostics of the laser plasma.

2.1. Generator of liquid-metal droplets

The generator of liquid-metal droplets incorporated the heated tank with liquid metal, equipped with the systems of vacuuming and gas (argon) supply under regulated pressure, as well as the capillary nozzle assembly, consisting of the nozzle and the porous filter. The tank of the droplet generator was made of 12X18H10T stainless steel that weakly interacts with the liquid tin and its eutectic alloys under the operational temperatures lower than 200°C. The nozzle was a silica capillary with the inner diameter 0.5 mm, tapered towards one of the ends. On the capillary the ring piezoelectric element (actuator) was mounted, by means of which the droplet generation was implemented. The electric capacity of the actuator amounted to 2–3 nF. The diameter of the nozzle outlet equalled a few tens of micrometres.

In the experiments two operation regimes of the nozzle were used, the droplet and the jet one. In the first regime in the tank the pressure of argon was sufficient to make a meniscus of liquid metal at the nozzle outlet, but insufficient to form a free jet. When a voltage pulse is applied to the piezoelectric element, the capillary cross section is increased or decreased depending on the voltage polarity, which leads to the change in pressure of the working medium in the capillary, i.e., to the formation of a compression-dilatation wave. The pressure wave propagates along the capillary towards the nozzle. At the nozzle outlet it is reflected from the liquid–vacuum boundary, thus transferring the momentum to the working medium, which leads to the droplet formation. Raising the pressure in the tank to the value, sufficient to overcome the capillary pressure, results in appearance of a jet, effluent from the nozzle. Thin jets of a liquid are characterised by the Rayleigh instability that leads to the disintegration of the jet into droplets at some distance from the nozzle, depending on the jet velocity. In this case, by applying voltage to the piezoelectric element one can forcedly modulate the jet disintegration.

Thus, the basic difference between these regimes is that in the droplet regime the droplets are not produced without the initiating pulse, while in the jet regime the pressure in the tank produces a freely disintegrating jet, which forms the droplets with a prescribed repetition rate under the modulation of the voltage applied to the piezoelectric element. Due to a higher pressure in the tank in the jet regime the velocity of droplets is higher (in our case nearly 8 m s^{-1}) than in the droplet regime (2–4 m s^{-1}). In the droplet regime to generate a droplet we usually used a bipolar initiating pulse, while in the jet regime the used pulses were unipolar. The signal amplitude in the droplet regime amounted to a few tens of volts, while in the jet regime it was a few volts, so that in the jet regime the nozzle operation in much less intensive, thus providing the prolonged lifetime of the piezoelectric ceramic element. To stabilise the operation of the droplet generator and to prevent the plugging of the nozzle, a porous filter made of zirconium or stainless steel with the size of the pores about 20 μm is installed between the tank and the nozzle. The tank and the nozzle assembly were equipped with a separate system of heating and temperature control. In the experiments as the working substance for droplets we used the eutectic alloy of indium (52 at %) and tin (48 at %) with the melting temperature 119°C. We use this alloy in our experiments because its physical properties are very close to the physical properties of tin, while the melting temperature is significantly lower than that of pure tin, due to which the alloy is less aggressive and more convenient in treatment. Besides, as shown in our experiments, in the EUV sources based on laser plasma the CE in the case of using the eutectic alloy is 70% of that for the pure tin. Thus, the use of the eutectic alloy as a model of the target working substance is justified.

2.2. Droplet diagnostics

The size of droplets, their velocity and spatial stability were determined using the method of shadow photography in a divergent light beam. The essence of the method consists in recording the shadow image of the droplets using the matrix of a CCD camera (*4*) (Fig. 1) in the light of the pulsed laser (*5*) flash, during which the droplet shift is negligible. As a diagnostic laser illuminating the droplets we used a diode laser with a wavelength 850 nm and pulse duration 30 ns. The uniformity of the illumination field was provided using an optical diffusor (*6*) with the scattering angle 20° and a positive lens (*7*). The microscope (*8*) and the objective (*9*) with a nearly twofold magnification projected the droplet image on the CCD matrix of the Manta MG-145B video camera.

To record the shadow photographs the background light was eliminated using a narrow-band filter (*10*) placed in front of the microscope with the transmission spectral width $\Delta\lambda = 850 \pm 5$ nm. The camera field of view had the size 4.7×3.5 mm; the spatial resolution was 3 μm. The optical resolution was determined by the pixel size of the camera (6.45 μm) and the magnification of the microscope and allowed the upper estimate of the target dispersity size (no larger than 3 μm). The maximal rate of recording the frames for the full size of the field of view was 15 Hz. The operation of the generator is stable if all droplets have the same velocity and flight trajectory. In the case of synchronous operation of the stable droplet generator and the illuminating pulsed laser, due to the stroboscopic effect, the image of the droplets displayed by the computer will be motionless. After recording a sequence of frames, we used the computer image

processing to study the stability of the droplet position at the time moment, determined by the diagnostic laser flash. The measurement was performed in two directions, the longitudinal one (along the vector of the droplet velocity) and the transverse one.

2.3. Femtosecond laser

The laser system consisted of a Tsunami master Ti:sapphire femtosecond oscillator (Spectra Physics) pumped by a Millennia Vs solid-state continuous-wave laser and a SpitFire Pro XP regenerative amplifier pumped by an Empower 30 pulsed solid-state laser. The system generated radiation in the range of wavelengths $\lambda = 800 \pm 20$ nm. The laser pulses had the Gaussian intensity profile in the transverse cross section. Using the lens (*7*) with the focal length 200 mm the caustic diameter of the laser radiation amounted to ~ 50 μm. The duration of the laser pulses could be varied in the wide range (half-width from 50 fs to 50 ps) and was determined at the half-maximum of the autocorrelation function using a Pulse Scout autocorrelator, the pulse energy of 2.3 mJ being constant. The pulse repetition rate was 1 kHz, so that to match the operation of the femtosecond laser and the CCD camera the frequency divider (*11*) was used that triggered the delay generator (*12*).

3. Synchronisation and alignment of the droplet generator

The pre-pulse technique in the EUV source based on laser plasma implies the use of a droplet target, stable in dimension and spatial position, with the standard deviation of the mass centre not exceeding 1%–2% of the droplet diameter. Taking into account the spot size of the focused laser radiation (50–100 μm) and the droplet size (30–50 μm), as well as the velocity of the droplet flight, in order to provide the stable hitting of the droplet by the laser beam in the experiment we used the multistep technology of synchronisation and alignment. We used two methods of hitting the droplet by the focused laser radiation. In the first one (see Fig. 1) the signal from the control unit of the femtosecond laser via the frequency divider was applied to the delay generator, which controlled the CCD camera via the first channel, the pulsed illuminating laser via the second channel, and the control unit of the droplet generator (*13*) via the third channel. By varying the delays between the pulse, initiating the control unit of the droplet generator and the flash of the diagnostic laser (and, therefore, the moment of opening of the CCD camera frame), one can get the droplet images at different moments of time after its exit from the nozzle. To aim the focused laser radiation at the trajectory of the droplet flight we used an auxiliary continuous-wave visible-range laser (*14*), whose optical axis was fit together with that of the pre-pulse laser, after which both radiations were aimed at the trajectory of the droplets flight. Then, by varying the delay of the pre-pulse laser triggering, the pulsed lasers were synchronised using the photodiodes (not shown in Fig. 1). At the last alignment stage the pre-pulse laser beam was finally corrected using the image of the droplet disintegration process in the CCD camera and a mirror to check the symmetry of the fragment separation picture with respect to the laser beam. Due to the jitter of the signal, controlling the nozzle, the pressure drift or temperature oscillations in the tank with liquid metal and the nozzle assembly, as well as the presence of mechanical particles in the working substance, the droplets can differ in velocity. That is why the second method of synchronisation, used by us in the experiments, in which the delay generator is triggered by the signal of scattering from the droplet, located slightly higher than the point of interaction between the laser pre-pulse and the drop, is more correct.

The triggering by the droplet was implemented using one more continuous-wave visible-range laser (*14*), the radiation of which was focused by the lens (*7*) on the axis of the droplet flight. In this case, the control unit of the droplet generator determined the rate of droplet generation. The droplet passing through the radiation beam of the continuous-wave laser produces scattering, and the scattered radiation is detected at a certain angle by the photodiode (*5*) (the duration of this pulse is $\Delta T = L/v$, where L is the size of the continuous-wave laser focal spot, and v is the droplet velocity). For correct operation of the synchronisation system ΔT should not exceed the period of droplet repetition. Via the transimpedance amplifier, the signal from the photodiode is applied to the signal maximum detector (*16*) (in Fig. 1 shown by a dashed line). By the moment of zero derivative of the signal, this device generates a pulse applied to the frequency divider. The frequency divider uses one channel to trigger the illuminating laser and the CCD camera via the delay generator. The other channel is used to trigger the pre-pulse laser. In this method of synchronisation, the droplet generator operates independently of other elements of the synchronisation scheme, and the frequency divider determines the frequency of interaction between the laser pulse and the droplet. We assume that in the operation regime of the EUV source incorporated in a lithography machine the frequency divider will not be used, and the laser will be triggered directly from the detector of the signal maximum. Because of the internal delays between the elements of the synchronisation scheme, almost 20 μs elapse from the moment of detecting the signal reflected from the droplet to the moment of generating the triggering signal for the diagnostic laser and the pre-pulse one. This time actually determines the stability of the droplet in the direction of its velocity vector. Indeed, if the velocities of the adjacent droplets differ only by 0.1 m s^{-1}, then the relative displacement of the droplets amounts to 3 μm, which for a droplet with the diameter 40 μm yields a 5% shift of the mass centre. Therefore, if the operation of the droplet generator is unstable, even the above synchronisation technique is unable to provide the required spatial stability ($\sigma = 1\%–2\%$).

4. Results and discussion

4.1. Operation of the droplet generator

Figures 2 and 3 present the shadow photographs of the droplets with the diameter ~ 60 μm in the droplet regime with the repetition rate $f = 5$ kHz and the jet regime with $f = 40$ kHz. In the droplet regime, the pressure of Ar in the tank with liquid metal was equal to ~30 mbar, and the velocity of the droplets amounted to 3 m s^{-1}. In the jet regime the respective values were 3.5 bar and 8 m s^{-1}. The maximal rate of droplet repetition, still allowing the stable operation of the droplet generator, was equal to 5 kHz in the droplet regime (for a droplet with the diameter 60 μm) and 150 kHz in the jet regime (for a droplet with

the diameter 30 μm). In the latter case, the maximal velocity of the droplets equal to 8 m s^{-1} limited the maximal repetition rate. The search for the stable regime of the generator operation consisted in careful adjustment of the droplet repetition rate, sometimes with the accuracy of a few hertz. At some repetition rates, we managed to get the spatial stability of the droplet position $\sigma \sim 1\,\%$ in both mutually perpendicular directions during more than an hour of operation. In the case of $f = 40$ kHz the separation between the droplets amounted to ~ 160 μm, so that for the caustic size of the laser radiation 50 μm or even 100 μm the laser beam did not touch the droplets adjacent to the working one.

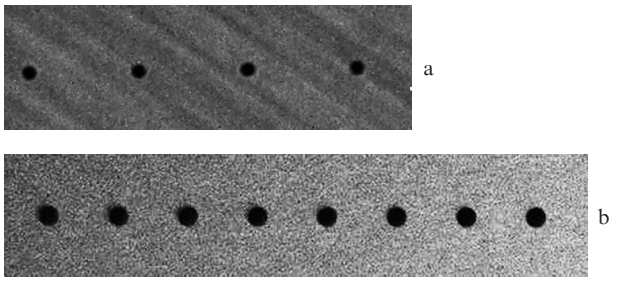

Figure 2. Shadow photographs of the droplets with the diameter 60 μm in (a) the droplet ($f = 5$ kHz) and (b) jet ($f = 40$ kHz) regimes.

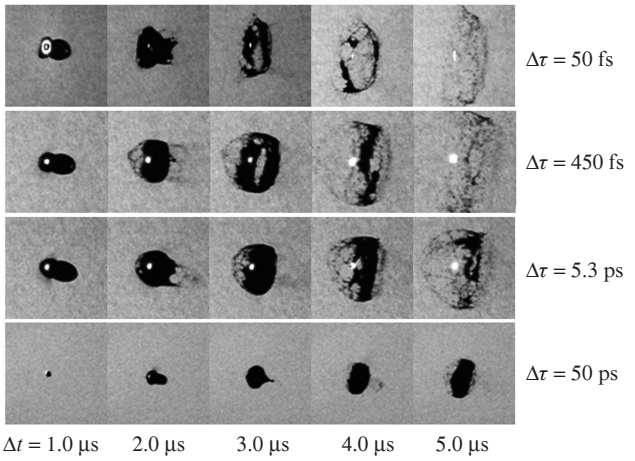

Figure 3. Shadow images of the deformation of a droplet with the diameter 60 μm (the frame size 1000 × 1000 μm) at different delays Δt with respect to the laser pulse of different duration $\Delta\tau$ (at the intensity half-maximum). The laser beam propagates from left to right at a small angle to the horizontal line.

In our experiments, we used the nozzles with different diameters of the capillary exit (from 20 to 40 μm). Usually the size of a droplet exceeded the size of the nozzle exit by 1.5 times; however, in some operation regimes of the droplet generator the adjacent droplets joined, and the droplet size appeared to be greater than expected. Finally, the droplet diameter varied from 30 to 70 μm. In the experiments on the study of droplet deformation under the action of femtosecond laser radiation, we mainly used the droplet regime of operation for the droplet generator with the repetition rate 8 Hz.

4.2. Droplet deformation under the action of a laser pulse

In the experiment we obtained the shadow photographs of the expanding droplet under the action of laser pulses of different duration $\Delta\tau$ of the femto- and picosecond range and with different delays Δt between these pulses and the illuminating laser pulse. For each pulse duration and all delays, a series of photographs was taken (no less than 160 frames). Each frame was processed using the computer programme that yielded the statistics of the position of the droplet centre of mass, the droplet size and velocity and the velocity of fragments flying away in different directions.

Figure 3 presents the shadow photographs of the droplets at different moments of time after the action of the laser pulses of different duration with the caustic diameter 50 μm. In addition to the laser pulse durations $\Delta\tau$ indicated in Fig. 3, the experiments were also performed with $\Delta\tau =$ 100 fs, 200 fs, 800 fs, 1.5 ps and 3 ps. The laser pulse in Fig. 3 propagates from left to right at a small angle to the horizontal direction. We see that in the course of time the droplet is transformed into a three-dimensional thin-wall shell of a complex dome-like shape, which is isotropically expanding. In 1 μs after the pulse action one can clearly see a structure with two expanding shells and a waist between them, the right shell expanding significantly faster than the left one.

As the shell expands, its thickness becomes smaller, and upon the achievement of a certain critical thickness, the shell begins to burst. It is seen that at $\Delta\tau$ from 50 fs to 5.3 ps the expansion pattern does not change qualitatively, while at $\Delta\tau =$ 50 ps the velocity of outgoing fragments sharply decreases. The light spot in the photographs corresponds to the luminous plasma. Assuming the centre of this spot to coincide with the initial position of the shells, one can determine their mean velocity at the time moment 1 μs. Figure 4 presents the dependences of the shell expansion velocities (in the direction of laser beam, in the opposite direction and in the transverse direction) on the laser pulse duration, plotted as a result of processing of the obtained frame sequences for the droplet with the diameter 60 μm and the caustic diameter 50 μm. Every point of the curves is a result of averaging over 100 frames. As seen from Fig. 4, the mean velocity of shell expansion amounts to ~ 300 m s^{-1} along the laser beam, nearly 80 m s^{-1} in the opposite direction, and about 120 m s^{-1} in the transverse direction. The dependence of the shell expansion velocity on the laser pulse duration in the direction of the laser beam has a pronounced maximum at the laser pulse duration 800 fs.

One can relate this experimental fact to the specific features of the mechanisms of laser radiation absorption. There are two competing mechanisms. On the one hand, according to [5], for an aluminium target the fraction of laser energy absorbed by the target within the range of laser power densities 10^{13}–10^{15} W cm^{-2} decreases with decreasing power density. On the other hand, due to a decrease in the electron density gradient at the boundary (because of the substance expansion) the fraction of laser energy absorbed by the target must grow with increasing pulse duration. As a result, at a certain pulse duration the maximum of the absorbed laser energy is possible. Hence, the dependence of the kinetic energy of the outgoing particles on the laser pulse duration can also have a maximum.

The optimal target size for the laser-plasma EUV source, determined by the size of the caustic of the main laser pulse (in

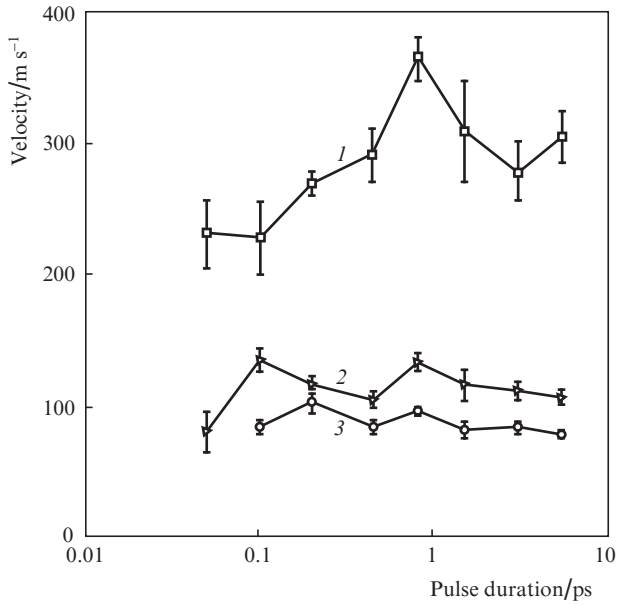

Figure 4. Dependences of the velocity of the target shell expansion on the pulse duration of the pre-pulse laser along the laser beam (*1*), in the perpendicular direction (*2*), in the direction opposite to the laser beam (*3*).

modern lithography machines this is usually a CO_2 laser) amounts to a few hundred micrometres. As seen from Fig. 3, in our experiments this size is achieved in 1.5–3 μs after the action of the pre-pulse laser.

For comparison with the above results we carried out the experiment with nanosecond radiation of the second harmonic of the Nd:YAG laser. The parameters of the laser pulse were as follows: the wavelength 532 nm, the pulse energy 15 mJ and the pulse duration 25 ns. Figure 5 shows the expansion of the fragments of a liquid-metal target with the diameter 60 μm made of the same eutectic In–Sn alloy in 1.5 μs after the action of the laser pulse. The laser beam is incident on the droplet from the left at a small angle to the horizontal line. As seen from Fig. 5, in this case, similar to [4], the character of the target fragmentation is qualitatively different from that in the case of femto- and picosecond pre-pulses. In particular, in the case of a nanosecond pulse the shape of the expanding shell is rather two-dimensional and resembles a planar disc with the edges bent in the direction of laser beam propagation.

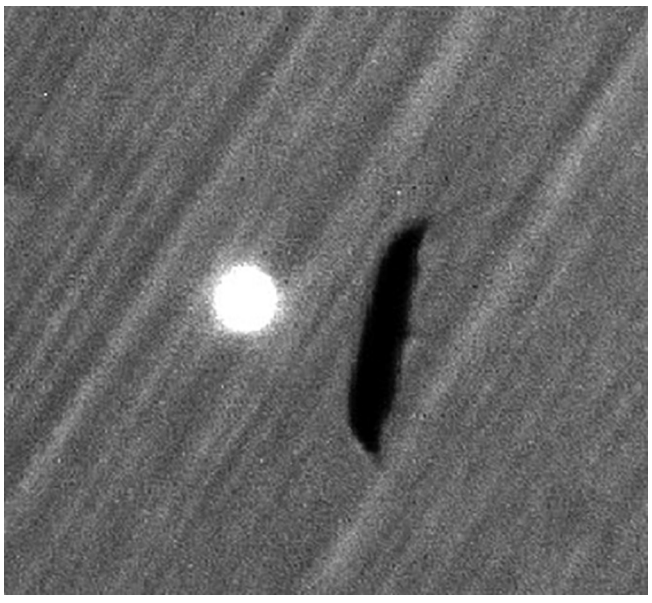

Figure 5. Shadow image of the deformed droplet with the diameter 60 μm (the frame size 600 × 550 μm); λ = 532 nm, the pulse energy 20 mJ, $\Delta\tau$ = 25 ns.

In further papers, we plan to present a more detailed discussion of the obtained results, including their comparison with the results of hydrodynamic calculation of the droplet expansion process under the action of a picosecond laser pulse and the results of the measurement of ion flow from the laser-produced plasma.

5. Conclusions

We have studied experimentally the process of fine-dispersed target formation by a laser pulse of femto- and picosecond duration within the frameworks of the pre-pulse technology for EUV sources based on the laser-produced plasma, used in the lithography systems of the newest generation. The fine-dispersed target resulted from the expansion of a droplet target consisting of the eutectic In–Sn alloy under the action of a laser pulse. The droplet disintegration was produced by the radiation of the Ti:sapphire laser with the pulse duration varied from 50 fs to 50 ps and the pulse energy of 2.3 mJ being constant. The maximal laser radiation power density at the target, averaged over the pulse duration and the spatial coordinates, amounted to 3×10^{15} W cm^{-2}.

It was found that within a wide range of laser pulse durations (from 50 fs to 50 ps) the dynamics of the droplet deformation is not changed. As a result of the interaction of the laser radiation and the droplet, a fine-dispersed three-dimensional target appears, the use of which, judging by the results of Ref. [4], will facilitate the achievement of high CE values in the EUV sources based on laser plasma.

The droplet generator based on a nozzle with a ring piezoceramic actuator is constructed. The generator can operate both in the droplet and jet regimes, differing by the maximal repetition rate and velocity of droplets. The maximal droplet repetition rate in the stable regime of the generator operation amounted to a few tens of kilohertz. The size of the droplets could be changed from 30 to 70 μm and the velocity from 2 to 8 m s^{-1}. We have developed two technologies of synchronising the laser radiation with fast flying droplet targets. The spatial stability of the droplet (1%–2% of its diameter) has been obtained both in the direction of the droplet motion and in the perpendicular direction for the droplet repetition rate up to 60 kHz.

Acknowledgements. The work was supported by the RF Ministry of Science and Education [Agreement No. 14.579.21.0004, unique identifier of applied scientific research (project) RFMEFI57914X0004].

References

1. Bakshi V. (Ed.) *EUV Source for Lithography* (Bellingham, Wash.: SPIE Press, 2006).

2. Banine V.Y., Koshelev K.N., Swinkels G.H.P.M. *J. Phys. D: Appl. Phys.*, **44**, 253001 (2011).
3. Hartlove J., Michaelian M., Shields H., Talmadge S., Fornaca S., Martos A. Patent US6973164, 30.12.2004.
4. Fujimoto J., Hori T., Yanagida T., Mizoguchi H. *Physics Research International*, **2012**, Article ID 249495 (2012).
5. Eliezer S. *The Interaction of High-Power Lasers with Plasmas*, (Bristol, Philadelphia: IOP Publ. Ltd, 2002).